Volume 11 | Number 15 | 21 April 2015 | Pages 2897–3084

Soft Matter

www.softmatter.org

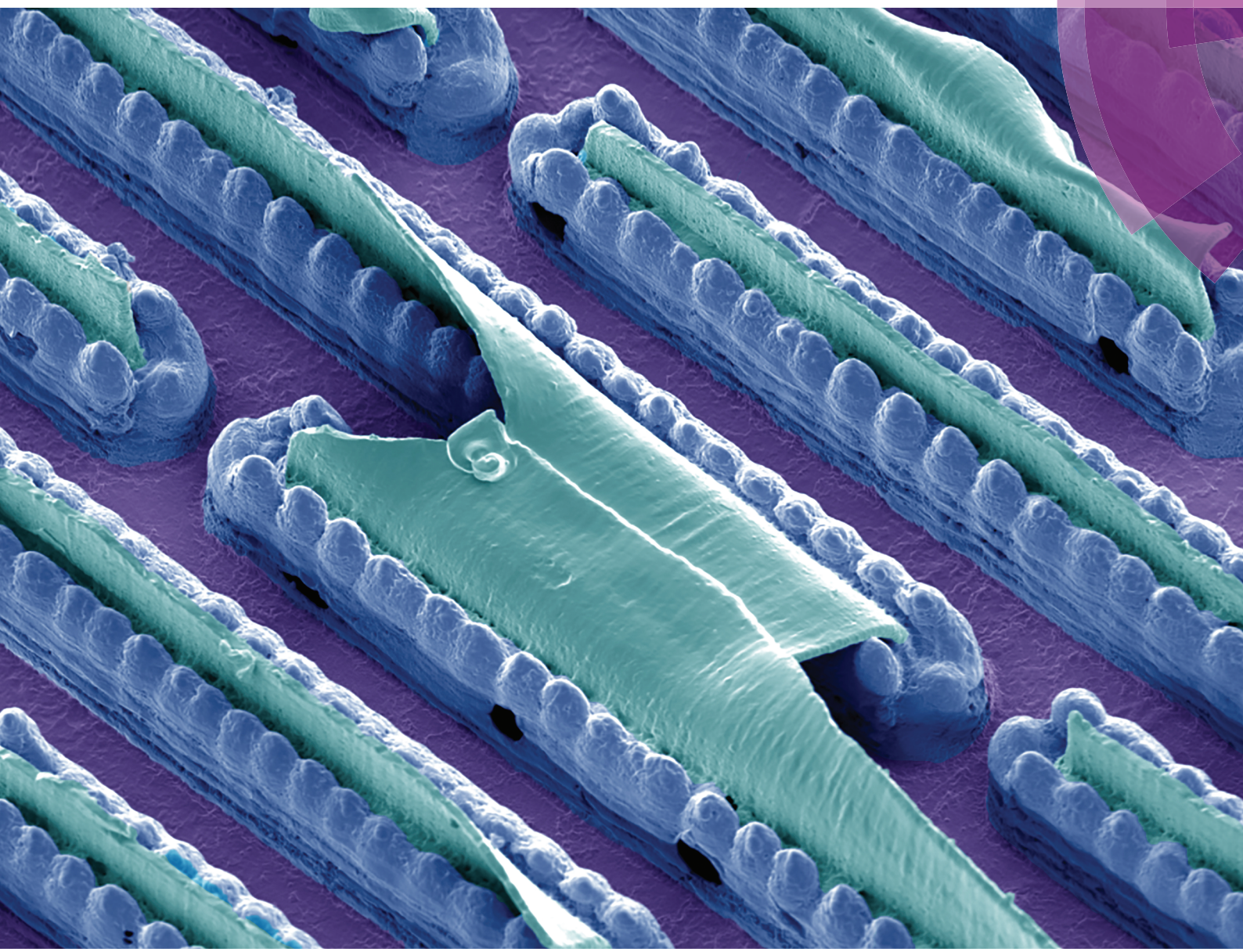

ISSN 1744-683X

ROYAL SOCIETY OF CHEMISTRY

PAPER
Michael Varenberg *et al.*
Biomimetic wall-shaped hierarchical microstructure for gecko-like attachment

Soft Matter

PAPER

View Article Online
View Journal | View Issue

Cite this: *Soft Matter*, 2015, **11**, 2909

Biomimetic wall-shaped hierarchical microstructure for gecko-like attachment

Haytam Kasem,[a] Alexey Tsipenyuk[a] and Michael Varenberg*[b]

Most biological hairy adhesive systems involved in locomotion rely on spatula-shaped terminal elements, whose operation has been actively studied during the last decade. However, though functional principles underlying their amazing performance are now well understood, due to technical difficulties in manufacturing the complex structure of hierarchical spatulate systems, a biomimetic surface structure featuring true shear-induced dynamic attachment still remains elusive. To try bridging this gap, a novel method of manufacturing gecko-like attachment surfaces is devised based on a laser-micromachining technology. This method overcomes the inherent disadvantages of photolithography techniques and opens wide perspectives for future production of gecko-like attachment systems. Advanced smart-performance surfaces featuring thin-film-based hierarchical shear-activated elements are fabricated and found capable of generating friction force of several tens of times the contact load, which makes a significant step forward towards a true gecko-like adhesive.

Received 27th August 2014
Accepted 10th February 2015

DOI: 10.1039/c4sm01916d

www.rsc.org/softmatter

Introduction

Hairy (fibrillar) attachment systems of insects, arachnids and reptiles have been intensively studied during the last decade,[1] aiming to reveal and possibly utilize functional principles underlying their amazing dynamical adhesive performance. These systems consist of arrays of hairs (setae) with two or more levels of hierarchy, which allow for a large contact area on almost any surface and hence feature high adhesion and friction derived from a combination of molecular interaction and capillary attractive forces.[2–7] The topmost hierarchical level of seta is responsible for the formation of intimate contact with the substrate and shows up as one or more terminal elements involving thin films.[8–12] In general, thin-film elements can be subdivided into two main groups characterized by different appearance and function. The thin-film elements of one type resemble mushroom caps (by protruding circumferentially from the seta stem) and are used for passive long-term attachment, such as in pairing, whereas the thin-film elements of the other type resemble spatulae (by protruding from the seta stem in one direction only) and are used for muscle-activated shear-induced short-term attachment required in locomotion.[13]

Based on the studies of different animal groups, an interesting correlation between the geometrical properties of setal tips and animal weight was found: the heavier the animal, the smaller and more densely packed the tips.[14] This scaling effect was explained by introducing the principle of contact splitting, according to which splitting up the contact into finer subcontacts increases adhesion,[15] which, based on its beauty and simplicity, has drawn an attention of many researchers. However, numerous attempts at employing this principle in manufacturing usable materials were surprisingly unsuccessful: in most cases, simple arrays of micropillars[16–22] have not exhibited a stronger adhesion than flat controls made of the same materials. Furthermore, it eventually appeared that the role of highly flexible terminal thin-film elements as compliant contacting surfaces is critical[23] and successful dry adhesive can hardly be constructed without these elements being involved.[24]

Earlier failures with simple micropillars have led many groups to start experimenting with thin-film terminal elements, and first truly working biomimetic adhesive was reported[25] after replicating mushroom-shaped attachment setae evolved in male beetles from the family Chrysomelidae. Mushroom-shaped structures were relatively easy to be fabricated due to their symmetry and thorough studies of their various properties and abilities have followed, performed first experimentally[21,26–41] and then theoretically.[42–45] However, though mushroom-shaped microstructure is well adapted for static passive applications such as glass safety coverings[46] or medical patches,[47] it is not able to withstand shear load, detach with zero load and respond directionally, which makes it not suitable for active dynamic short-term attachment required in many cases.

Considering the fact that most biological hairy attachment systems involved in locomotion actually rely on spatula-shaped terminal elements,[13] the spatulate systems were also studied, though the results achieved are mainly related to theoretical rationalizations. Preceded by pioneer work on peeling of thin-films,[48] the principles underlying the spectacular performance

[a]*Dept. of Mechanical Engineering, Technion, Haifa 32000, Israel*
[b]*George W. Woodruff School of Mechanical Engineering, Georgia Institute of Technology, Atlanta, GA 30332, USA. E-mail: varenberg@gatech.edu*

of biological spatula-shaped fibrillar attachment systems are continuously uncovered,[7,12,49–59] opening the way to further advance. However, due to technical difficulties in manufacturing the complex hierarchical structure of adhesion-driven spatulate systems, there were only a few attempts to study them experimentally[60–64] and the progress made is limited. To try bridging this gap, here we report on a manufacturing method and a novel smart-performance surface design featuring thin-film hierarchical shear-activated elements capable of generating friction force of several tens of times the contact load, which makes a step forward towards a true gecko-like adhesive.

Results and discussion

Fabrication

A set of problems that had to be faced in order to manufacture thin-film-based hierarchical shear-activated surface elements and the solutions we suggest are summarized in Table 1. The main points are these.

(1) As long as the counter surface is smooth, splitting the attachment pad in parallel to the horizontal component of the peeling force does not enhance the attachment ability,[57] so there is no need in pillar-based projections that were invariably used so far. Instead, we propose wall-shaped projections, whose lengths (dimension in perpendicular to the horizontal component of the peeling force) are much larger than their widths and heights. In addition to easier fabrication due to smaller number of contact elements, this also allows more efficient use of available contact area and longer total peeling line length, which was found to govern biological fibrillar adhesion.[57]

(2) As long as soft elastomers are used, thin films are involved and shear motion is necessary to actuate the system, there is no need in making surface projections slanted, as they are flexible enough to build good contact without much elastic energy being stored. This allows making them essentially perpendicular to the contact plane, which significantly simplifies fabrication. Interestingly, even in relatively stiff keratin-based biological attachment systems, terminal spatulate plates are oriented in perpendicular to the contact plane,[61,65] which confirms our approach.

(3) It is well known that biological adhesive hairs become thinner towards their ends,[10,12,66] which suggests that thickness gradients have to be built into the artificial systems as well. Photolithography methods used widely in fabrication of biomimetic adhesives are, however, hardly capable of imparting such feature into the design of surface projections. To this end, here we suggest using laser machining in preparing casting templates, which allows creating gradients by adjusting the laser beam geometry. In addition to (a) ability of cutting depressions with a depth-dependent width, other advantages of using laser machining instead of photolithography methods are (b) ability to machine non-flat templates, such as rolls that can be used in continuous mass production, (c) practical lack of limitation in treated area, (d) ability to machine thin metal sheets that are much more robust in handling than brittle silicon wafers, and (e) ability to obtain smaller surface roughness of deep cut walls.

(4) Given that in an unloaded wall-shaped projection the working surface is perpendicular and not parallel to the contact plane, we suggest making the template depressions as deep as possible and using fast-polymerizing elastomers for creating structured surfaces. This allows fabricating wall-shaped hierarchical projections of different heights using the same template by adjusting the dwell time between mixing and pouring the polymer, which solidifies before reaching the bottom of the template.

(5) Given that there is no need to fill the template completely, it can consist of through slots instead of blind depressions. Openings at the back side of the template simplify the fabrication process significantly by preventing air trapping during the template filling, easing the cast release and facilitating the template cleaning.

Based on the above guidelines, we have manufactured two types of wall-shaped hierarchical microstructures using two different laser-machined templates (Fig. 1 and Table 2, see Experimental section for details). The main difference between the two types of projections is in the form of the projection base, whose section resembles a crown in one case and a triangle in the other case. In fact, the crown base was not planned originally and appeared as a laser-cutting artefact during a first attempt to produce a casting template. The problem was resolved by adjusting the process parameters in the following attempts. Fig. 1d and f–h demonstrates that this approach indeed allows fabricating wall-shaped hierarchical microstructures with bases of gradually changing thickness and thin-film terminal elements of different heights.

Table 1 Manufacturing guidelines

Problem	Solution
Increasing total peeling line length without increasing the number of projections	Use of long wall-shaped projections instead of pillars with effectively circular cross section
Ease of template fabrication & cast release	Making wall-shaped projections essentially perpendicular to the contact plane
Securing gradients in projection width	Use of laser machining for template fabrication
Control of projection height	Use of fast-polymerizing elastomer that can solidify before reaching the bottom of template
Prevention of air trapping during the template filling & ease of cast release	Use of template with through slots instead of blind depressions

Measurements

Fig. 2 presents the behavior of wall-shaped hierarchical microstructures loaded in normal and tangential directions. Interestingly, both types of microstructures were found to be easily detachable and non-sticky by default, which corresponds well to

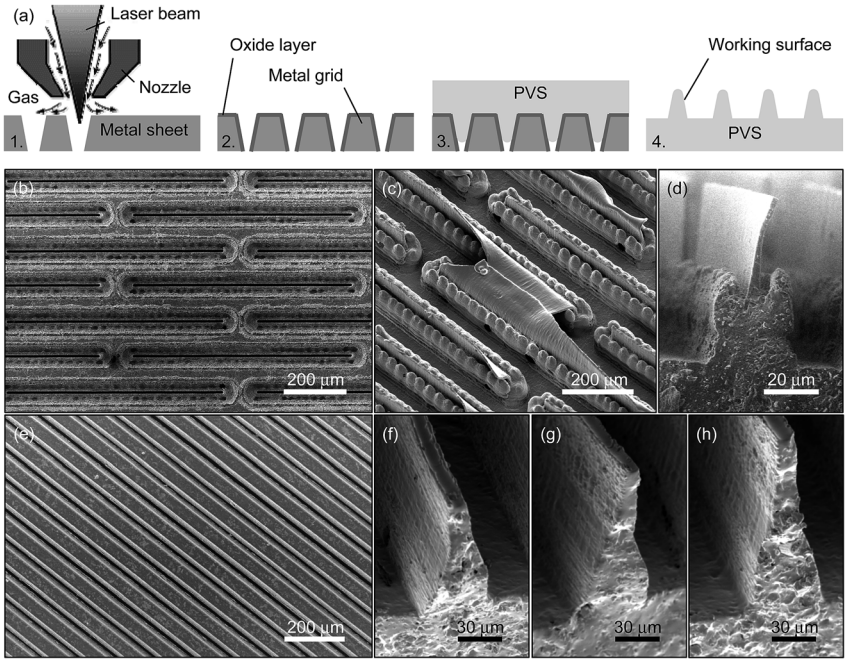

Fig. 1 Fabrication of wall-shaped hierarchical microstructures. (a) Schematic of manufacturing process. 1. Laser machining of casting template. 2. Surface treatment for easier cast release. 3. Casting. 4. Releasing the ready-to-use cast. (b) Plan view of the entry side of the tungsten template for casting microstructures with crown base. (c) Angled view of the microstructured elastomer surface bearing projections with crown base. (d) Side view of single hierarchical elastomeric projection with crown base. (e) Plan view of the entry side of the tungsten template for casting microstructures with triangular base. (f), (g), (h) Side views of single hierarchical elastomeric projections with triangular bases and various flap heights.

their biological prototypes.[60] This is explained by the following reason. The surface projections are perpendicular to the contact plane and, when loaded in a normal direction only, they buckle randomly (Fig. 2a). Deformed elastically, they store elastic energy that is recovered during the surface withdrawal as reaction contact forces that act against adhesion and lead to negligible externally applied load known as pull-off force (Fig. 2d). This effect becomes even more pronounced due to a non-simultaneous detachment of the wall-shaped projections, which do not share the same height as a result of casting into a template without a bottom.

The picture changes completely when the normally loaded projections are subjected to shear. Initially randomly buckled projections are gradually sheared to take similar shape under the growing tangential load. They stretch, overturn and eventually all get oriented in the same direction (Fig. 2b and c), which allows them acting in concert against the external tangential load. This unites contributions of single thin-film microstructures and makes them capable of generating stable and unusually high friction force of up to several tens of times the normal load at the onset of sliding (Fig. 2e). Withdrawing the wall-shaped microstructures in normal direction on completion of tangential motion, we have learned that simple detachment that follows shearing stage leads to increase in peeling angle and, in accord with analysis of biological attachment systems,[7] to negligible detachment force. Thus, in order to study the directional performance of the wall-shaped microstructure, it is first necessary to enable application of peeling force at constant angle, which is planned for the future.

Maximum friction force obtained at the onset of sliding was determined for all tested surfaces. These data are presented in Fig. 3, where the performance of both types of wall-shaped hierarchical microstructures is shown. It can be seen that the slope of the friction force *vs.* normal load curve, which is the "true" friction coefficient,[67] is similar in all cases except that of the triangular-based microstructure bearing medium flaps, which demonstrated different slope at the normal loads of less than 10 mN (shown as filled triangular markers). Interestingly, the above generic slope of the friction force *vs.* normal load curve characterizes not only the microstructured surfaces but

Table 2 Geometry of wall-shaped hierarchical microstructures studied in this work

Base type	Base height, μm	Base width, μm	Flap height, μm	Flap edge width, μm	Projection length, μm	Projection pitch, μm
Crown	80	90	80	6	750	150
Triangular	70	50	25	12	Sample-size	95
—	—	—	40	12	—	—
—	—	—	70	11	—	—

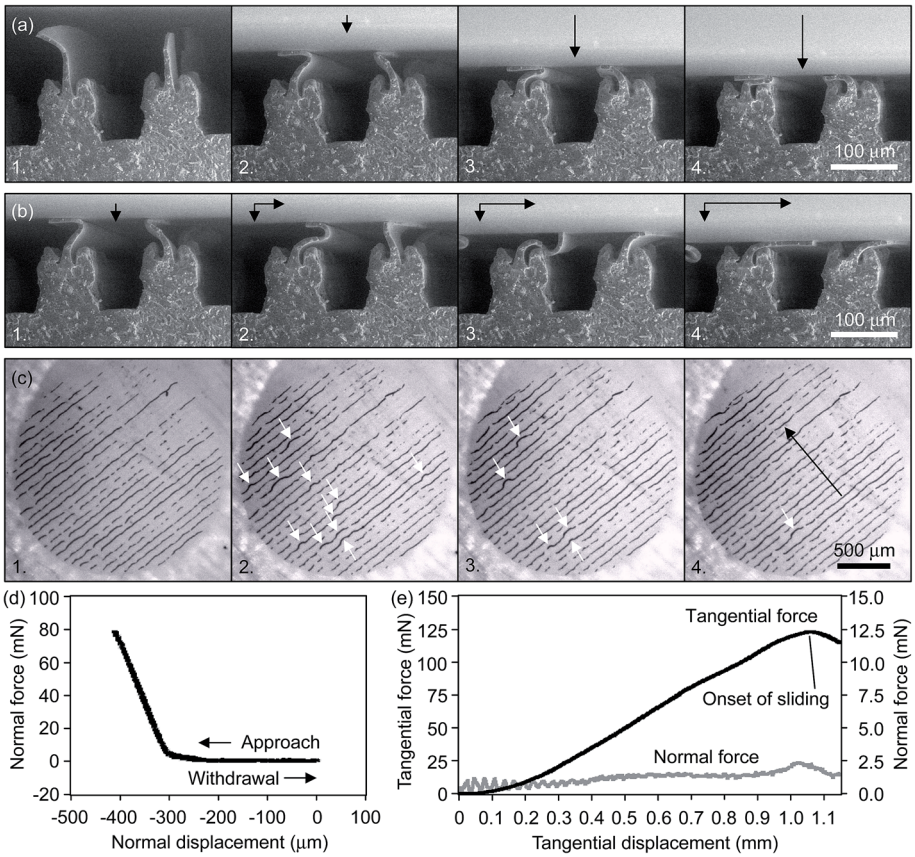

Fig. 2 Behavior of wall-shaped hierarchical microstructures loaded in normal and tangential directions. (a) A microstructure with crown base under the increasing normal load. Arrows in the direction of load. (b) A microstructure with crown base brought to the onset of sliding (in frame 4) under the increasing tangential load, while the normal load does not change. Arrows in the direction of load. (c) Real contact area formed by a microstructure with a triangular base and visualized as dark lines by a destructive interference of white light. 1. Initial contact under the normal load only. 2–4. Overturning of the microstructure flaps from one side to another in the course of tangential load increase. Black arrow points in the direction of the specimen motion. White arrows point to the areas where flaps are not yet overturned. (d) Pull-off force curve obtained on a microstructure with a triangular base. (e) Friction force curve obtained on a microstructure with a triangular base and high flaps. Normal force controlled in closed loop to keep it constant is shown for reference.

also the smooth reference (ring lying on its flat side, see Experimental section for details), whose frictional performance correlates well with that reported earlier for the samples having the same geometry and made of the same material.[68] This points out that knowing friction coefficient is not enough to evaluate friction force, as it can be offset significantly by changing the surface geometry.

Comparing the frictional performance of triangular-based microstructures, we can suggest that there is an optimum flap height with which a maximum friction force is obtained. This is explained as follows. Based on the peel-zone model developed for pressure-sensitive adhesives but applicable also to a dry adhesion case,[54] we can conclude that if a thin-film flap is not high enough, the real contact area is narrower than a possible active peel zone (defined by a balance of elastic, adhesive and frictional energies) to allow high attachment force. On the other hand, if the flap is too high, then, when in contact with the mating surface, it can interfere with the neighbor projections once they are close enough, which again handicaps overall attachment (most likely it was also the case of the crown-based microstructure that had the highest flaps). Somewhere in between the two extreme cases, however, there is an optimum in the flap height, which should be defined by the peel zone width and the surface projections pitch. This assumption is yet to be further verified.

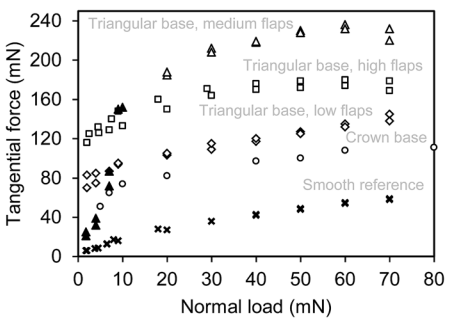

Fig. 3 Tangential force at the onset of sliding (static friction force) presented as a function of normal load in hierarchical microstructured surfaces with crown bases (○) as well as triangular bases bearing high (□), medium (Δ) and low (◇) flaps. Performance of smooth surface (×) is given for reference.

Coming back to the slope of the friction *vs.* load curve obtained with the medium flaps of the triangular-based microstructure at the normal loads of less than 10 mN (see filled triangular markers in Fig. 3), we can propose the following possible reason for it being significantly different from those obtained under other conditions. To allow for self-aligning required to bring flat surfaces in complete contact, both specimens are fixed on tense orthogonal threads[68] that are twisted when the surfaces coming in contact are not parallel, which necessitates a certain load. Most likely, in the discussed case the surfaces were initially not parallel, which resulted in that not all wall-shaped hierarchical projections yet came in contact at normal loads of less than 10 mN and hence led to low friction. Thus, the observed result is identified as a measurement artefact.

It is also worth trying to evaluate the progress of the present work, including the manufacturing method itself and the frictional performance of the surfaces made, in comparison to the previous studies on spatulate attachment microstructures.[60–64] In template preparation, the present technique seems to be easier as it is based on a straightforward two-step laser machining (first, cutting blind trenches and, then, cutting through slots at the trench bottoms) of a commercially available metal sheet that can be used for a virtually infinite number of casts. The photolithography techniques used previously are more complicated as they are based on several-step procedures including various materials and chemicals, and most of the templates are limited to about 10 casts. In casting the microstructured surfaces, the present technique also seems to be easier as it allows working in air at room temperature, as long as the photolithography-based techniques require casting under vacuum and heat curing.

Comparison of frictional performance is not so simple, as in most cases the test conditions differ significantly. However, given that the largest ratio of friction force to normal load is obtained at light loads, the present microstructure performs seemingly better with the friction to load ratio of 50 (Fig. 2e) as opposed to that of 3 ÷ 16 obtained with previously reported spatulate microstructures having architectures of wedge-shaped[60,61,64] and flap-shaped pillars.[62,63] Direct comparison is possible only with ref. 64, where a friction force of 400 mN was obtained with a 12.6 mm^2 area sample under the normal load of 25 mN. The present study reports a friction force of 200 mN obtained with a 3.14 mm^2 area sample under the same normal load, which gives a two-fold better result.

Conclusion

We have devised a novel method of manufacturing gecko-like hierarchical shear-activated attachment surfaces based on laser micromachining. This method overcomes the inherent disadvantages of photolithography techniques and opens wide perspectives for future production of low-cost gecko-like attachment systems. Advanced surfaces we have fabricated are found capable of generating friction force of several tens of times the contact load, while exhibiting optimum geometrical properties presumably determined by interrelations between the height and pitch of surface elements. This presents a further progress in comparison to the previously reported achievements and makes a significant step forward towards a true gecko-like adhesive.

Experimental

Specimens, preparations and conditions

Four types of hierarchical microstructured surfaces were cast from poly(vinylsiloxane) (PVS; Coltène Whaledent AG, Altstätten, Switzerland) using two negative templates produced by laser micro-machining (Oxford Lasers, Oxon, UK) from 0.15 mm-thick tungsten sheets to have through slots of different sizes. To allow easier cast release, the tungsten templates were oxidized in Ozone PSD-II Probe Cleaner (Novascan Technologies, Ames, IA) for 30 min. The height of individual surface projections was controlled by the dwell time of 30, 60 and 90 s between mixing and pouring the PVS onto the template, while the curing time of PVS is about 3 min when its two components are stored at room temperature before mixing. The cast thickness was controlled by using spacers between the template and a covering flat surface. The cast release was done in a water bath after a 30 min stay in ultrasonic cleaner. Microstructured side of the cast was used for contact surface of bio-inspired specimens, while smooth flat side of the same cast was used for contact surface of reference specimens. Structured and reference smooth samples of 2 mm in diameter were punched out of the same 1 mm-height PVS cast (Young's modulus of about 3 MPa)[19] using disposable biopsy Uni-Punch (Premier Products Co., Plymouth Meeting, Pennsylvania). Based on that the real contact area of structured samples is much smaller than the apparent area of the sample (Fig. 2c), it was decided to have comparable real contact area in both structured and reference smooth samples. To this purpose, the center area of the smooth sample (disk of 2 mm in diameter and 1 mm in height) was removed to form a ring of outer diameter of 2 mm, inner diameter of 1 mm and height of about 0.2 mm. The central depression was first cut with a 1 mm-in-diameter punch and then removed with a sharp knife. Contact area of structured and reference smooth samples had roughness average, R_a, of 760 and 541 nm, respectively. The structured PVS samples were mounted in such a way as to orient the surface projections in perpendicular to the sliding direction. The tests were performed in contact with smooth (R_a = 5 nm) glass slide of 30 × 5 × 1 mm^3 in size. The temperature and relative humidity in the laboratory were 20–22 °C and 40–50%, respectively. The pressure inside the scanning electron microscope (SEM) vacuum chamber was 300 Pa.

Equipment

Surface appearance of the specimens used was inspected with an optical stereomicroscope Leica M125 (Leica GmbH, Wetzlar, Germany) and imaged in a FEI Quanta 200 environmental SEM (FEI Co., Brno, Czech Republic). The tests were performed on a home-made tribometer[69] capable of operating inside the environmental SEM to enable charge-free imaging of non-

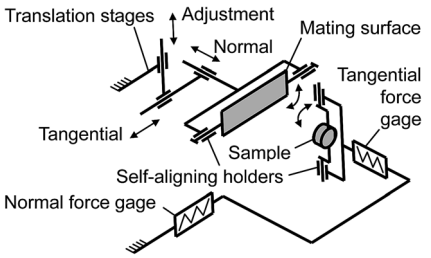

Fig. 4 Schematic of the experimental set-up.

conductive uncoated PVS specimens. The tribometer (Fig. 4) incorporates two main units used for driving and measuring purposes. The drive unit consists of three motorized translation stages used to load the contact by moving the glass specimen. The measurement unit consists of two load cells used to determine the forces acting on the PVS specimen. The load cells are fixed in that way that normal force acts in the plane in which tangential load cell is not sensitive, and tangential force acts in the plane in which normal load cell is not sensitive, thus preventing cross-talk between force sensors (Fig. 4). To guarantee full contact and fulfil the 'equal load sharing' principle[18] during force measurements in a flat-on-flat contact scheme essential in surface texture testing, a passive self-aligning system of specimen holders was used.[68] In order to examine the microstructure behavior in contact, the contact area was imaged with a monochrome digital camera UI-1240LE (IDS Imaging Development Systems, Germany) enhanced by high-magnification optics Zoom-12X (Navitar Inc., Rochester, New York).

Procedure

All specimens were tested in the following way. Adhesion tests were done by bringing the glass specimen in contact with the PVS specimen and then, after applying a normal load of 80 mN, withdrawing the translation stage in the normal direction at a velocity of 100 μm s^{-1} while measuring the pull-off force. In friction tests, after bringing the specimens in contact and applying a normal load chosen between 2 and 80 mN, the translation stage was moved in the lateral direction at a velocity of 100 μm s^{-1} for a distance of 1200 μm with the normal load being kept constant, while the friction force resisting the specimen motion was recorded. Immediately on completion of lateral motion, the translation stage was withdrawn in a normal direction at a velocity of 100 μm s^{-1} and the pull-off force affected by shearing was also measured. During the experiments carried out inside SEM, the translation stages were moved incrementally and, following each incremental displacement, the contact projections were imaged with SEM to examine visually their gradual deformation. Each PVS specimen was tested at every load on a different region of the glass specimen and then replaced. Prior to experiments, the specimens were washed with deionized water and liquid soap, and then dried in blowing nitrogen.

Acknowledgements

This work was supported by the Technion V. P. R. Fund, the Jewish Communities of Germany Research Fund, the Russell Berrie Nanotechnology Institute and the Israeli Ministry of Economy (METRO 450 Consortium within the frame of MAGNET program) to M. V. H. K. was supported by The Center for Absorption in Science, Ministry of Immigrant Absorption, State of Israel.

Notes and references

1 M. Zhou, N. Pesika, H. Zeng, Y. Tian and J. Israelachvili, *Friction*, 2013, **1**, 114–129.
2 K. Autumn, Y. A. Liang, S. T. Hsieh, W. Zesch, W. P. Chan, T. W. Kenny, R. Fearing and R. J. Full, *Nature*, 2000, **405**, 681–685.
3 K. Autumn, M. Sitti, Y. C. A. Liang, A. M. Peattie, W. R. Hansen, S. Sponberg, T. W. Kenny, R. Fearing, J. N. Israelachvili and R. J. Full, *Proc. Natl. Acad. Sci. U. S. A.*, 2002, **99**, 12252–12256.
4 B. N. J. Persson, *J. Chem. Phys.*, 2003, **118**, 7614–7621.
5 M. G. Langer, J. P. Ruppersberg and S. Gorb, *Proc. R. Soc. London, Ser. B*, 2004, **271**, 2209–2215.
6 G. Huber, H. Mantz, R. Spolenak, K. Mecke, K. Jacobs, S. N. Gorb and E. Arzt, *Proc. Natl. Acad. Sci. U. S. A.*, 2005, **102**, 16293–16296.
7 Y. Tian, N. Pesika, H. Zeng, K. Rosenberg, B. Zhao, P. McGuiggan, K. Autumn and J. Israelachvili, *Proc. Natl. Acad. Sci. U. S. A.*, 2006, **103**, 19320–19325.
8 N. E. Stork, *J. Linn. Soc. London, Zool.*, 1980, **68**, 173–306.
9 N. E. Stork, *J. Nat. Hist.*, 1983, **17**, 583–597.
10 S. N. Gorb, *Proc. R. Soc. London, Ser. B*, 1998, **265**, 747–752.
11 S. N. Gorb, *Attachment Devices of Insect Cuticle*, Kluwer Academic, Dordrecht, 2001.
12 B. N. J. Persson and S. N. Gorb, *J. Chem. Phys.*, 2003, **119**, 11437–11444.
13 S. N. Gorb and M. Varenberg, *J. Adhes. Sci. Technol.*, 2007, **21**, 1175–1183.
14 M. Scherge and S. N. Gorb, *Biological Micro- and Nanotribology: Nature's Solutions*, Springer, Berlin, 2001.
15 E. Arzt, S. Gorb and R. Spolenak, *Proc. Natl. Acad. Sci. U. S. A.*, 2003, **100**, 10603–10606.
16 M. Sitti and R. S. Fearing, *J. Adhes. Sci. Technol.*, 2003, **17**, 1055–1073.
17 N. J. Glassmaker, A. Jagota, C.-Y. Hui and J. Kim, *J. R. Soc., Interface*, 2004, **1**, 23–33.
18 C.-Y. Hui, N. J. Glassmaker, T. Tang and A. Jagota, *J. R. Soc., Interface*, 2004, **1**, 35–48.
19 A. Peressadko and S. N. Gorb, *J. Adhes.*, 2004, **80**, 247–261.
20 B. Aksak, M. P. Murphy and M. Sitti, *Langmuir*, 2007, **23**, 3322–3332.
21 A. del Campo, C. Greiner and E. Arzt, *Langmuir*, 2007, **23**, 10235–10243.
22 C. Greiner, A. del Campo and E. Arzt, *Langmuir*, 2007, **23**, 3495–3502.

23 N. J. Glassmaker, A. Jagota, C. Y. Hui, W. L. Noderer and M. K. Chaudhury, *Proc. Natl. Acad. Sci. U. S. A.*, 2007, **104**, 10786–10791.
24 M. Varenberg, B. Murarash, Y. Kligerman and S. Gorb, *Appl. Phys. A*, 2011, **103**, 933–938.
25 K. A. Daltorio, S. Gorb, A. Peressadko, A. D. Horchler, R. E. Ritzmann and R. D. Quinn, in *CLAWAR*, London, 2005.
26 S. Kim and M. Sitti, *Appl. Phys. Lett.*, 2006, **89**, 261911.
27 B. Bhushan and R. A. Sayer, *Microsyst. Technol.*, 2007, **13**, 71–78.
28 S. Gorb, M. Varenberg, A. Peressadko and J. Tuma, *J. R. Soc., Interface*, 2007, **4**, 271–275.
29 S. Kim, B. Aksak and M. Sitti, *Appl. Phys. Lett.*, 2007, **91**, 221913.
30 M. P. Murphy, B. Aksak and M. Sitti, *J. Adhes. Sci. Technol.*, 2007, **21**, 1281–1296.
31 M. P. Murphy, B. Aksak and M. Sitti, *Small*, 2009, **5**, 170–175.
32 M. P. Murphy, S. Kim and M. Sitti, *ACS Appl. Mater. Interfaces*, 2009, **1**, 849–855.
33 M. Varenberg and S. Gorb, *J. R. Soc., Interface*, 2007, **4**, 721–725.
34 M. Varenberg and S. Gorb, *J. R. Soc., Interface*, 2008, **5**, 383–385.
35 M. Varenberg and S. Gorb, *J. R. Soc., Interface*, 2008, **5**, 785–789.
36 P. Glass, H. Y. Chung, N. R. Washburn and M. Sitti, *Langmuir*, 2010, **26**, 17357–17362.
37 E. Cheung and M. Sitti, *J. Adhes.*, 2011, **87**, 547–557.
38 L. Heepe, M. Varenberg, Y. Itovich and S. Gorb, *J. R. Soc., Interface*, 2011, **8**, 585–589.
39 M. K. Kwak, H. E. Jeong, W. G. Bae, H.-S. Jung and K. Y. Suh, *Small*, 2011, **7**, 2296–2300.
40 A. Kovalev, M. Varenberg and S. Gorb, *Soft Matter*, 2012, **8**, 3560–3566.
41 H. Kasem and M. Varenberg, *J. R. Soc., Interface*, 2013, **10**, 20130620.
42 A. V. Spuskanyuk, R. M. McMeeking, V. S. Deshpande and E. Arzt, *Acta Biomater.*, 2008, **4**, 1669–1676.
43 G. Carbone, E. Pierro and S. N. Gorb, *Soft Matter*, 2011, **7**, 5545–5552.
44 G. Carbone and E. Pierro, *Small*, 2012, **8**, 1449–1454.
45 L. Heepe, G. Carbone, E. Pierro, A. E. Kovalev and S. N. Gorb, *Appl. Phys. Lett.*, 2014, **104**, 011906.
46 S. N. Gorb, 2011, private communication.
47 M. K. Kwak, H. E. Jeong and K. Y. Suh, *Adv. Mater.*, 2011, **23**, 3949–3953.
48 K. Kendall, *J. Phys. D: Appl. Phys.*, 1975, **8**, 1449–1452.
49 A. E. Filippov and V. L. Popov, *Tech. Phys. Lett.*, 2005, **31**, 871–874.
50 R. Spolenak, S. Gorb, H. Gao and E. Arzt, *Proc. Math. Phys. Eng. Sci.*, 2005, **461**, 305–319.
51 A. E. Filippov and V. L. Popov, *J. Phys.: Condens. Matter*, 2007, **19**, 096012.
52 B. N. J. Persson, *J. Adhes. Sci. Technol.*, 2007, **21**, 1145–1173.
53 B. N. J. Persson, *MRS Bull.*, 2007, **32**, 486–490.
54 N. S. Pesika, Y. Tian, B. X. Zhao, K. Rosenberg, H. B. Zeng, P. McGuiggan, K. Autumn and J. N. Israelachvili, *J. Adhes.*, 2007, **83**, 383–401.
55 B. Chen, P. D. Wu and H. Gao, *Proc. Math. Phys. Eng. Sci.*, 2008, **464**, 305–319.
56 B. Chen, P. Wu and H. Gao, *J. R. Soc., Interface*, 2009, **6**, 529–537.
57 M. Varenberg, N. Pugno and S. Gorb, *Soft Matter*, 2010, **6**, 3269–3272.
58 A. Filippov, V. L. Popov and S. N. Gorb, *J. Theor. Biol.*, 2011, **276**, 126–131.
59 L. Afferrante, G. Carbone, G. Demelio and N. Pugno, *Tribol. Lett.*, 2013, **52**, 439–447.
60 A. Parness, D. Soto, N. Esparza, N. Gravish, M. Wilkinson, K. Autumn and M. Cutkosky, *J. R. Soc., Interface*, 2009, **6**, 1223–1232.
61 N. Gravish, M. Wilkinson, S. Sponberg, A. Parness, N. Esparza, D. Soto, T. Yamaguchi, M. Broide, M. Cutkosky, C. Creton and K. Autumn, *J. R. Soc., Interface*, 2010, **7**, 259–269.
62 J. Yu, S. Chary, S. Das, J. Tamelier, N. S. Pesika, K. L. Turner and J. N. Israelachvili, *Adv. Funct. Mater.*, 2011, **21**, 3010–3018.
63 K. Jin, Y. Tian, J. S. Erickson, J. Puthoff, K. Autumn and N. S. Pesika, *Langmuir*, 2012, **28**, 5737–5742.
64 S. Chary, J. Tamelier and K. Turner, *Smart Mater. Struct.*, 2013, **22**, 025013.
65 D. Voigt, J. M. Schuppert, S. Dattinger and S. N. Gorb, *J. Insect Physiol.*, 2008, **54**, 765–776.
66 T. Eimüller, P. Guttmann and S. N. Gorb, *J. Exp. Biol.*, 2008, **211**, 1958–1963.
67 B. V. Derjaguin and Y. P. Toporov, *Prog. Surf. Sci.*, 1994, **45**, 317–327.
68 M. Varenberg, A. Peressadko, S. Gorb, E. Arzt and S. Mrotzek, *Rev. Sci. Instrum.*, 2006, **77**, 066105.
69 B. Murarash and M. Varenberg, *Tribol. Lett.*, 2011, **41**, 319–323.